LAWRENCE
LIVERMORE
NATIONAL
LABORATORY

UCRL-PROC-221772

X-ray Digital Radiography and Computed Tomography of ICF and HEDP Materials, Subassemblies and Targets

W. D. Brown, H. E. Martz Jr.

June 1, 2006

Digital Imaging IX
Mashantucket, CT, United States
July 24, 2006 through July 26, 2006

X-ray Digital Radiography and Computed Tomography of ICF and HEDP Materials, Subassemblies and Targets

William D. Brown, Harry E. Martz, Jr.
Lawrence Livermore National Laboratory
7000 East Ave., Livermore, CA 94551, USA

INTRODUCTION

Inertial confinement fusion (ICF) and high energy density physics (HEDP) research are being conducted at large laser facilities, such as the University of Rochester's Laboratory for Laser Energetics OMEGA facility and the Lawrence Livermore National Laboratory's (LLNL) National Ignition Facility (NIF). At such facilities, millimeter-sized targets with micrometer structures are studied in a variety of hydrodynamic, radiation transport, equation-of-state, inertial confinement fusion and high-energy density experiments. The extreme temperatures and pressures achieved in these experiments make the results susceptible to imperfections in the fabricated targets.[1,2] Targets include materials varying widely in composition ($\sim 3 < Z < \sim 82$), density (~0.03 to ~20 g/cm^3), geometry (planar to spherical) and embedded structures (joints to subassemblies). Fabricating these targets with structures to the tolerances required is a challenging engineering problem the ICF[3] and HEDP[4] community are currently undertaking. Nondestructive characterization (NDC) provides a valuable tool in material selection, component inspection, and the final pre-shot assemblies' inspection.[5] X-rays are a key method used to NDC these targets. In this paper we discuss X-ray attenuation, X-ray phase effects, and the X-ray system used, its performance and application to characterize low-temperature Raleigh-Taylor and non-cryogenic double-shell targets.

CONSEQUENCES OF μm X-RAY RADIOGRAPHY AND COMPUTED TOMOGRAPHY

The size, wide mass density and elemental range of these targets limits the utility of traditional X-ray attenuation radiography. The high Z and high density of some materials used in these targets require X-ray energies of about 60 keV to penetrate the target. However, micrometer-scale structures and small density differences within the target often produce low-contrast in X-ray attenuation radiographs. In addition, traditional X-ray sources have spot sizes that are too large to adequately resolve micrometer-scale structures. The size of ICF and HEDP targets, and the materials that comprise them lead us to the use of micro-focus or synchrotron X-ray sources in the 5 to 100 keV energy range. With the high-spatial coherence of the micro-focus and synchrotron X-ray sources and the high-spatial-resolution detectors employed, image contrast due to the wave nature of the X-rays, is manifested in the radiographic data, sometimes termed X-ray phase-contrast imaging. Propagation of an electromagnetic wave field through free-space can render phase effects visible in the measured irradiance distribution. Historically, X-ray radiography and computed tomography (CT) have been performed assuming that the X-rays are either attenuated or transmitted, but not deflected (i.e., Compton scattered, refracted or diffracted) from their path. The X-ray-wave phase change is responsible for refraction and diffraction of the X-rays, just as with visible light. However, the phase change can be used to render visible low-attenuation structures.[6] The fact that phase effects are observed in our data demonstrates that the basic assumption for conventional X-ray radiography and radiographic simulation, and X-ray tomography and tomographic reconstructions, namely, that the X-rays follow straight paths, is violated.[7]

X-RAY RADIOGRAPHIC AND TOMOGRAPHIC SYSTEM

We employed an X-ray point-projection system developed by Xradia Inc. called Micro-XCT.[8] This system uses a Hamamatsu tungsten-anode source with a nominal spot size of 5 micrometers at 4 watts and a maximum potential of 150 kV. The detector is a 25-μm CsI scintillator microscope (10X and 20X) lens coupled to a 16-bit Andor Charged-Coupled-Device (CCD) camera. The CCD chip is 2048x2048, with a detector-element pitch of 13.5 μm X 13.5 μm. It was operated at -50°C in the experiments reported here.

In order to begin quantifying the digital radiography (DR) and computed tomography system performance, Modulation Transfer Functions (MTF) and Signal-to-Noise Ratios (SNR) were measured. DR system performance was obtained using a tungsten roll-bar or edge.[9] Transmission (I/I_0) images were created and an edge response of the system was obtained from a lineout across the tungsten edge. The derivative of the lineout is taken resulting in the edge response or line-spread function (LSF) of the X-ray system. A Fourier transform of the LSF results in the MTF. The MTF is a frequency domain description of the spatial resolution of the X-ray system. The DR MTF's for the Xradia 10x and 20X objective lenses are presented in Figure 1. The DR MTF values at 20% modulation for the 10 and 20X objectives are 110 and 175 lp/mm, respectively.

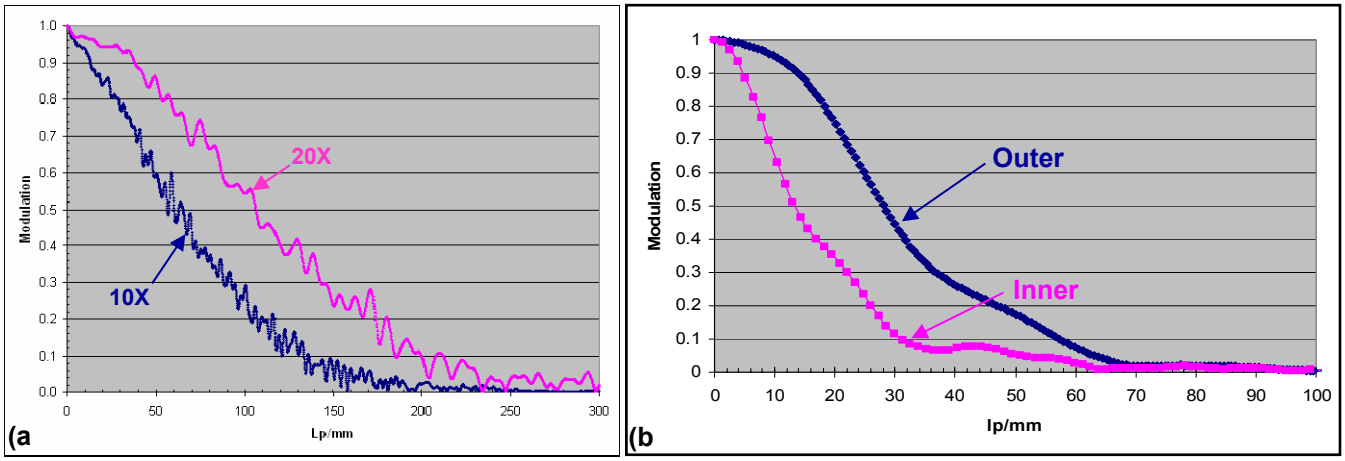

Figure 1: Tungsten-edge Micro-XCT DR MTFs (a) and KCAT Au tube-wall CT MTFs (b).

The tungsten roll-bar is also used to derive the SNR for the DR system. The SNR is given by $(S_1-S_2)/[(\sigma_1^2 + \sigma_2^2)^{½}]$, where S is the mean of the signal and σ is the standard deviation of the signal. The SNR's for the Micro-XCT 10X and 20X objectives are 155 and 110, respectively. The SNR for the 10X objective is 29% greater than the 20X objective.

To calculate CT MTF's, we acquired three tubes of different materials (low-density polystyrene, Cu and Au) and dimensions.[10] Here we only describe the Au tube. The Au tube was specified with an outer diameter of 0.300 mm and a wall thickness of 0.050 mm. The tubes were scanned on a Lawrence Livermore developed system called KCAT that had a pixel size of 3 μm at the center of each tube. The DRs were converted to sinograms, ring removal and beam hardening corrections were applied to each sinogram before reconstructed using a convolution back projection algorithm. 1D profiles (lineouts) were obtained across the outer (OD) and inner (ID) diameter for each tube wall and processed to derive the KCAT OD and ID MTFs, respectively (Figure 1). KCAT's OD MTFs are somewhat similar to KCAT's DR MTFs. The ID MTFs have a lower MTF at the corresponding frequency of the OD MTFs as expected primarily due to X-ray scatter by the object.

CHARACTERIZATION OF LOW-TEMPERATURE RALEIGH-TAYLOR TARGETS

Low-temperature Raleigh-Taylor (LoTRT) targets are used in a new laser-driven technique to produce dynamic, shockless compression of materials for studying the properties of matter at high pressure and density, but low temperature.[11] This work is based on the conversion of kinetic energy into thermal pressure. This is applicable to planetary science, measurement of solid-state dynamics at ultrahigh strain rates relevant to meteor impact and crater formation studies, and for equation of state studies and interstellar dust dynamics. A LoTRT target consists of a number of solid and hollow disks with various materials including a Au shield, a LiF window, an Al coating, a CH ablator, a Br-doped CH reservoir and a gradient density SU8 reservoir.

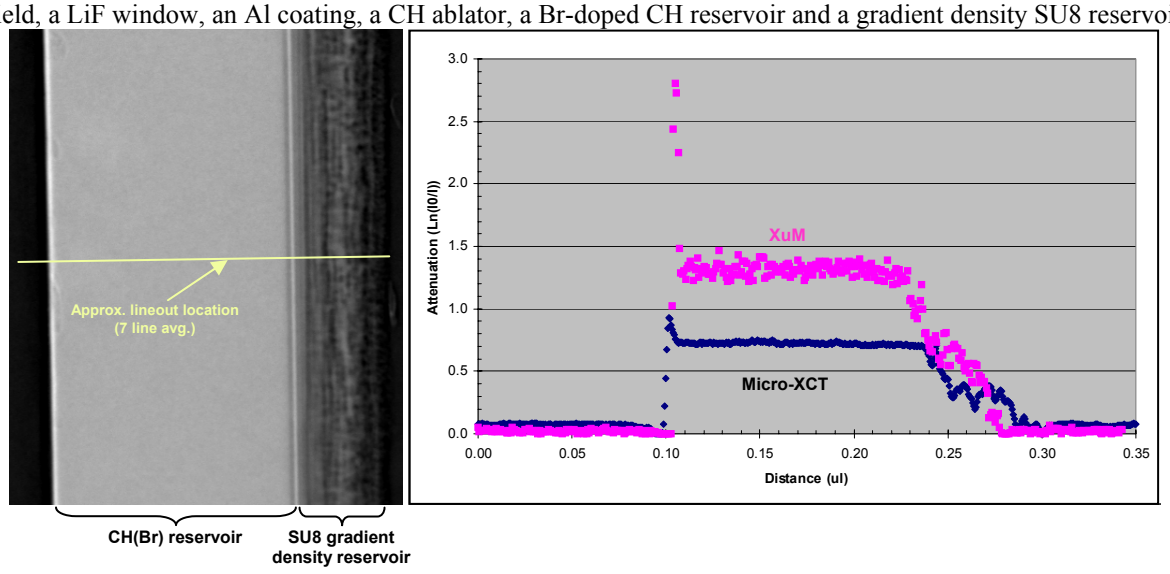

Figure 2: Representative Micro-XCT attenuation DR, and Micro-XCT and XuM profiles of the CH(Br) and SU8-gradient-density reservoirs. XuM is an X-ray Ultra-Microscopy system developed by XRT Limited.

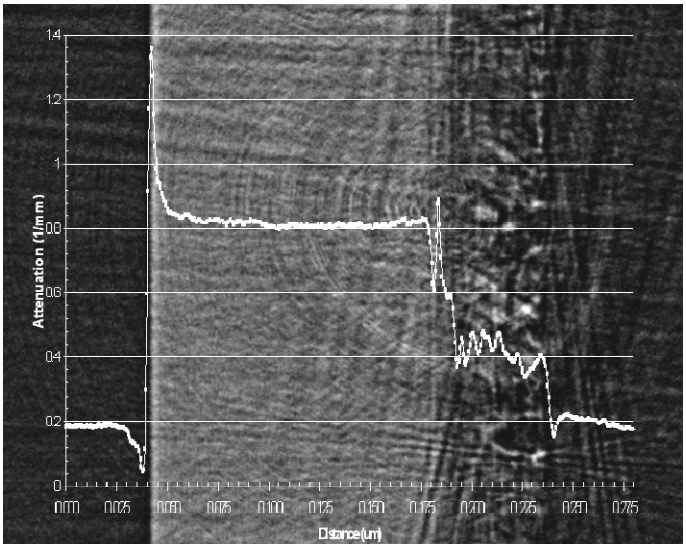

Figure 3: CH(Br) and SU8-gradient-density reservoirs Micro-XCT CT *x,y* cross section with a *y,z* profile overlay.

The gradient density SU8 reservoir is a newly developed sub-assembly component that is very difficult to fabricate and characterize.[12] The SU8 reservoir contains 60 layers of SU8 photoresist with density varying roughly from 0.2 to 1.2 g/cm^3.

To characterize the SU8 density gradient both DR and CT were acquired with 100-kV potential and 0.04-mA current. Source-to-object and object-to-detector distances of ~61 and ~14 mm, respectively were employed resulting in a pixel pitch of 0.6 μm at the target center and data acquisition times of ~2 minutes per DR; 720 views were acquired for CT image reconstruction. Due to the 60 layers of SU8, the DR (Figure 2) and CT (Figure 3) data contain X-ray refraction or phase effects at each boundary as well as the conventional X-ray attenuation effects. X-ray phase effects are revealed in the images as bright and dark regions at each layer interface. These effects interfere with the attenuation data and make it difficult to measure the density gradient in the SU8 material. We have modeled the SU8 reservoir with phase effects and we plan on using the model to better understand the gradient density in the SU8 material.[12]

CHARACTERIZATION OF NON-CRYOGENIC DOUBLE-SHELL TARGETS

A complementary approach to cryogenic deuterium-tritium filled single-shell targets demonstrating ignition uses non-cryogenic double-shell (DS) targets.[13] The DS target ignition tolerance to interface instabilities is rather low, thus the characterization requirements are particularly strict. For example, in a double-shell target the outer spherical shell is assembled from two hemi-shells with a glued step joint that requires mating within a few hundred nanometers and an inner and outer delta radius of less than 1.0 μm.[4] Concentricity of inner and outer shells to within 3 μm, sphericity of each shell, wall thicknesses of each shell, material uniformity and wicking of glue into foams are other issues that must be characterized since they can affect the hydrodynamics of the as-built target.

A double shell (DS) target consists of two concentric shells. The outer shell is a CH(Br-doped) ablator with inner and outer diameter of 444 and 550 μm, respectively. The inner shell is made of glass with an outer diameter of 216 μm and wall thickness of 8 μm. The inner shell is held in place within the outer shell 50 mg/cm^3 SiO_2 aerogel. In the first DS target manufacturing campaign the aerogel was machined as two hemi-shells with a cavity to house the inner shell concentric to the outer. The outside diameter of the aerogel was machined slightly less than the ID of the ablator. To construct the double shell target, the lower aerogel hemi-shell was placed in the lower ablator and the glass shell was mounted in the machined cavity of the lower aerogel (Figure 4). The upper aerogel hemi-shell is then placed on the lower aerogel hemi-shell and the upper ablator hemi-shell was placed over the lower assembly and glued. A final machining of the outer diameter ablator was performed to meet specifications. During the first campaign (December 2004 and January 2005) a total of six DS targets were fabricated.

Both digital radiography (Figure 4) and computed tomography (Figure 5) were used to characterize the double shell targets. Typical source-to-object and object-to-detector distances of ~119 and ~12, mm, respectively were employed resulting in a pixel pitch of 0.6 μm at the target and data acquisition times of 60 seconds per DR; 360 views were acquired for the CT image reconstruction. During review of the DRs, a void between the upper and lower aerogel hemi-shells was detected (Figure 4). The void appeared to be wedge-shaped in the digital radiographs and was confirmed in some but not all

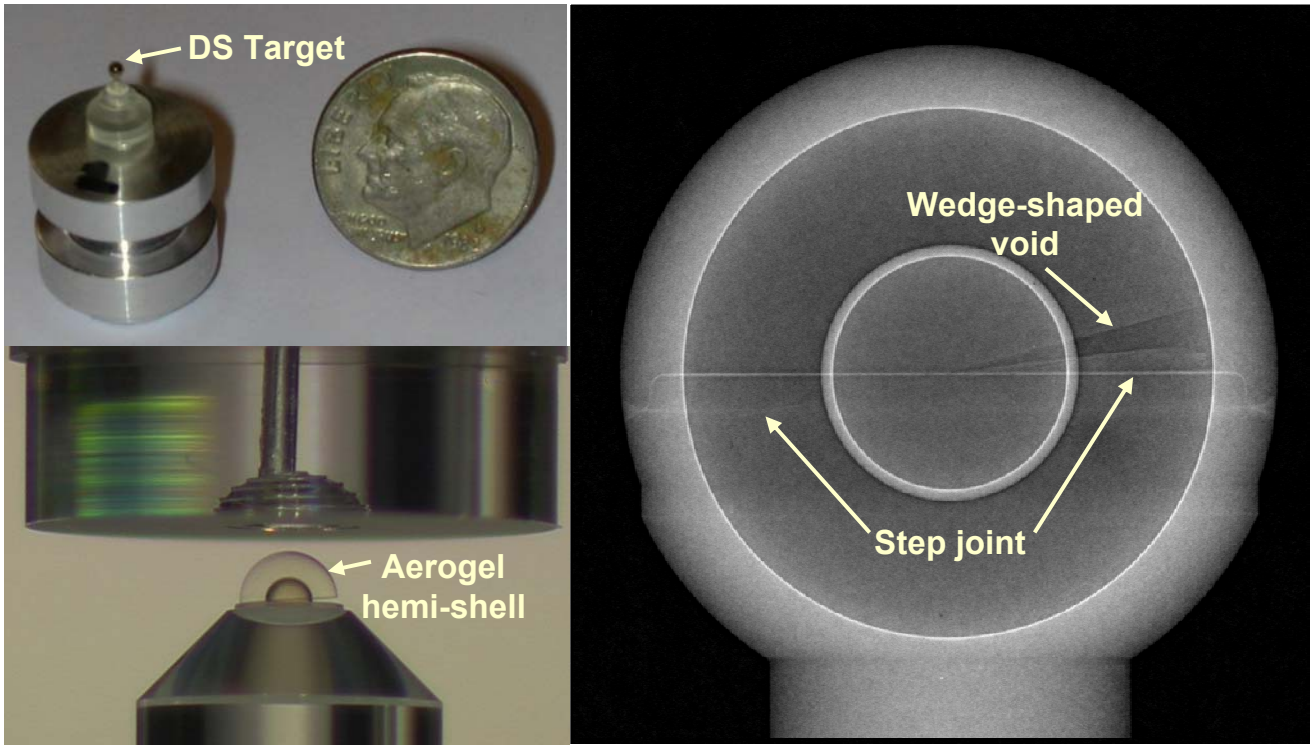

Figure 4: First build DS target final assembly photograph (top left), photograph during assembly (bottom left) and Micro-XCT DR (right) showing the wedge-shaped void/gap and the glued step joint in the outer ablator shell.

of the CT images. Characterization of all six targets revealed similar wedge-shaped voids. CT revealed that the six targets had inner shell to outer shell concentricity ranging from 0.5 to 1.7 μm,[14] well within the 3 μm specification. Three of the six targets had ablator wall thickness uniformity met the physicist's request of 1 μm or better, the other 3 targets ranged from 1.7 to 3.9 μm thus do not meet this uniformity. [14] DR also revealed step discontinuities in excess of 1 μm on the inner surface of the ablator for a few of the targets. Consequently, the manufacturing process had to be changed for future double shell targets.

The new double shell target manufacturing involved casting the inner glass shell within SiO_2 aerogel and then machining the aerogel to the ID ablator specifications. A cast was made and partially filled with sol, a precursor to SiO_2 aerogel, and left to condense. Before the sol fully condensed to a gel, an inner shell was placed in the aerogel solution submerging about half of the shell. Additional solution was added to the cast, fully encasing the glass shell. After the gel was supercritically extracted to form aerogel, DR and CT shown in Figures 6 and 7, respectively, were used to verify that there were no

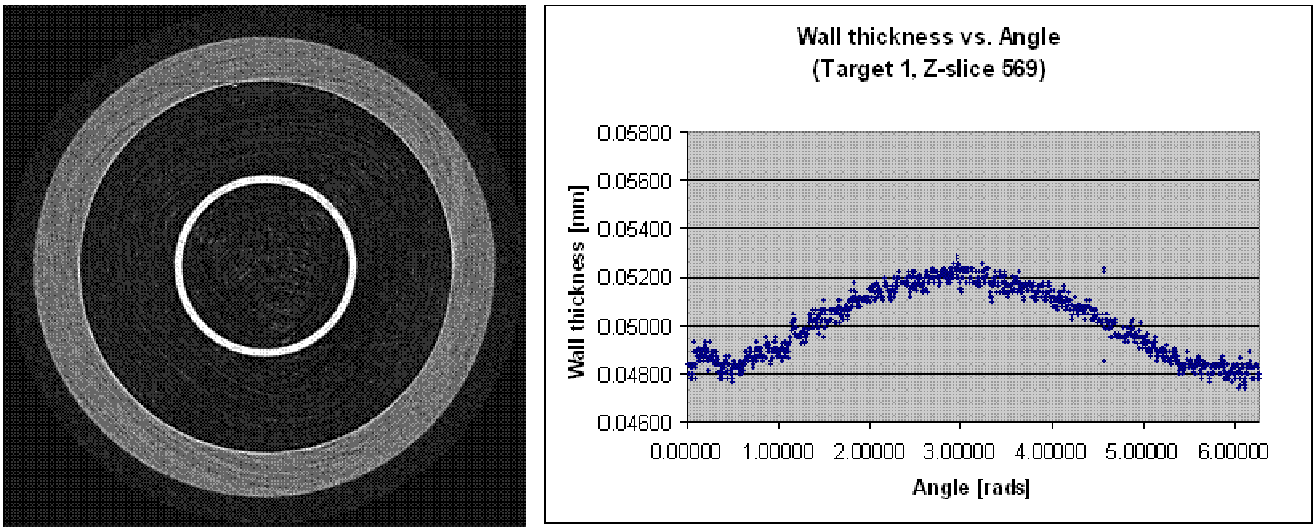

Figure 5: DS target 1 *x,y* cross section CT image (left) and wall thickness vs. angle measurement (right) for this image.

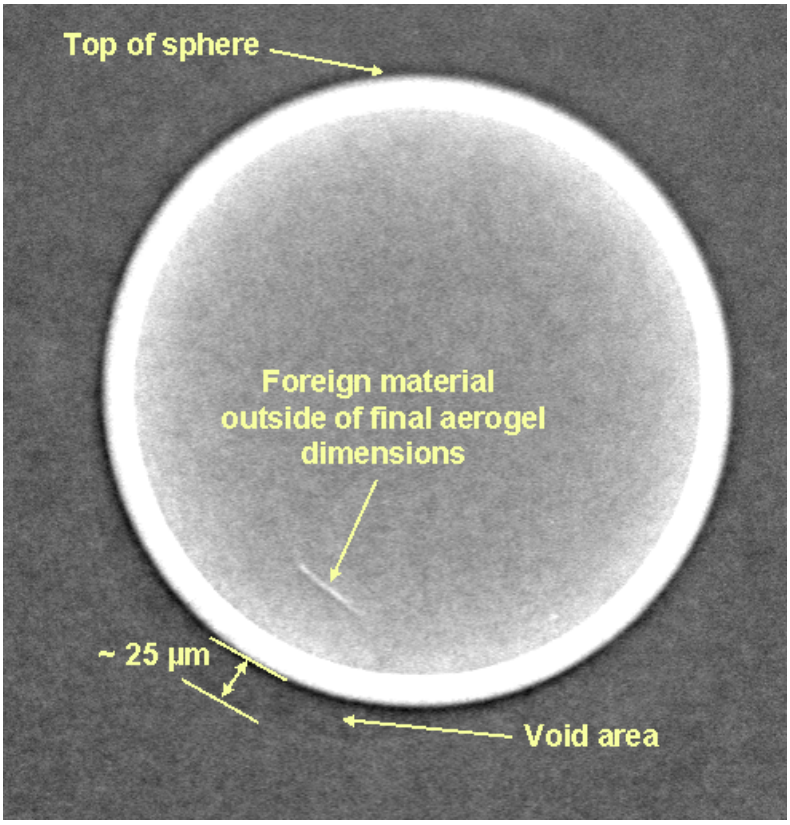

Figure 6: DR of DS target 5 reveals inclusion and voids in the aerogel casting.

inclusions or voids within the cast aerogel. If the data showed no voids or inclusion, the aerogel/shell casting was sent for final machining. The final aerogel/shell machined sub-assembly was placed in the lower ablator and the upper hemi-shell ablator was placed on the lower assembly and glued. Final machining of the outer diameter ablator was performed before final inspection. A first article double shell target was assembled in March 2006 using the new design method. Again, both DR and CT were used to characterize the new DS first article. After review of the DR and CT data, there were no wedge-shaped voids within the aerogel as seen before in the first campaign of DS targets.

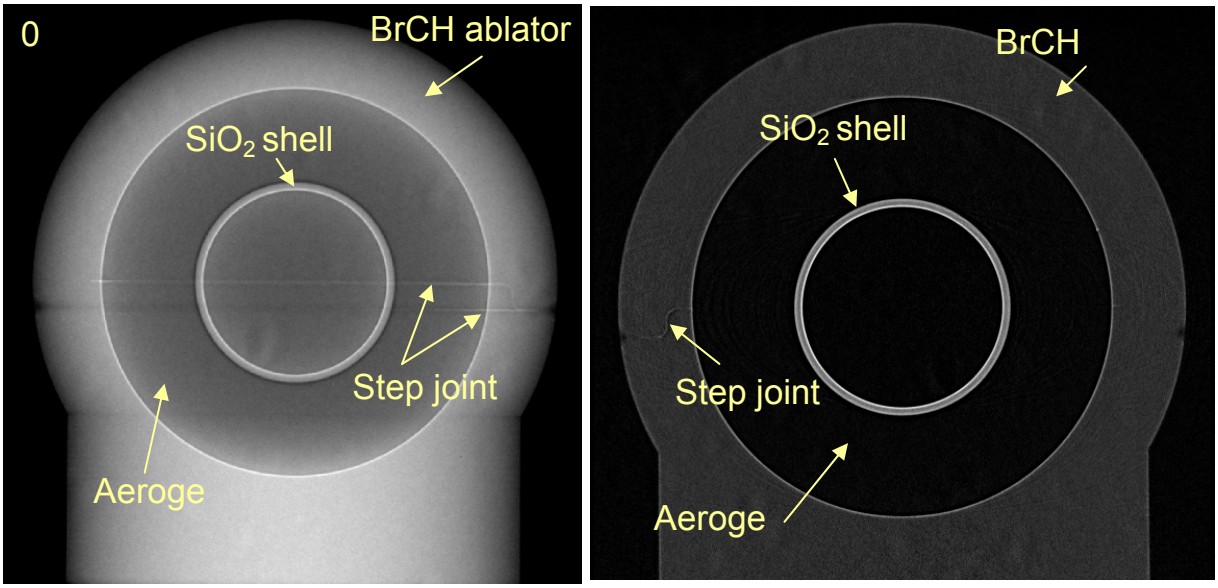

Figure 7: DR (left) and CT (right) images of second manufacturing campaign DS target first article.

SUMMARY

ICF and HEDP targets require sub-micrometer spatial resolution characterization. When X-ray DR and CT are employed with micrometer spatial resolution X-ray refraction (or phase) effects are observed in the data. These so-called phase effects make it difficult to interpret the X-ray DR and CT data. We are exploring models to help interpret such data. A high spatial resolution (pixel pitch at the object of 0.6 μm) X-ray system developed by Xradia Inc., Micro-XCT, performance was characterized by DR MTFs and SNRs. The DR MTF values at 20% modulation for the 10 and 20X objectives are 110 and 175 lp/mm, respectively. The SNR's for the Micro-XCT 10X and 20X objectives are 155 and 110, respectively.

This system was used to begin to characterize gradient density reservoirs for low-temperature Raleigh-Taylor and non-cryogenic double-shell targets. Work is still under investigation to better determine the gradient density in the reservoirs. In the first DS target manufacturing campaign wedge-shaped voids were observed in the DR and CT data. In addition, CT revealed that the six targets had inner shell to outer shell concentricity ranging from 0.5 to 1.7 μm, well within the 3 μm specification. Three of the six targets had ablator wall thickness uniformity met the physicist's request of 1 μm or better, the other 3 targets ranged from 1.7 to 3.9 μm and did not meet this uniformity. DR also revealed step discontinuities in excess of 1 μm on the inner surface of the ablator for a few of the targets. Consequently, the manufacturing process had to be changed for future double shell targets. A second DS target manufacturing campaign is underway to meet double shell target specifications. Preliminary X-ray DR and CT results reveal that these DS targets may meet the design specification.

ACKNOWLEDGMENTS

We thank John Sain for help in the data analysis of the double shell targets. Matt Bono has been instrumental in helping us understand the double shell target design specifications. We thank Clint Logan for his comments on this report. This work was performed under the auspices of the U.S Department of Energy by the University of California, Lawrence Livermore National Laboratory under Contract No. W-7405-Eng-48.

REFERENCES

1. Lindl, J. D., *Intertial Confinement Fusion*, (Springer-Verlag, New York, 1998).
2. Haan, S. W., et al., "Update on NIF Indirect Drive Ignition Target Fabrication Specifications," *Fusion Science and Technology*, **45**, 69-73 (2004).
3. Sater, J., et al., "Cryogenic D-T Fuel Layers Formed in 1 mm Spheres by Beta-Layering," *Phys. Rev. B*, **35**, 1482-1491 (1998).
4. Hibbard, R. L., et al., "Precision Manufacturing of Inertial Confinement Fusion Double Shell Laser Targets for OMEGA," *Fusion Science and Technology*, **45**, No. 2, 117-123 (2004).
5. Martz Jr., H. E. and Albrecht, G. F., "Nondestructive Characterization Technologies for Metrology of Micro/Mesoscale Assemblies," in *Proceedings of: Machines and Processes for Micro-scale and Meso-scale Fabrication, Metrology, and Assembly*, (American Society for Precision Engineering, Raleigh, NC, 2003) pp. 131-141.
6. Wilkins, S. W., et al., "Phase-contrast imaging using polychromatic hard X-rays," *Nature*, **384**, 335-338 (1996).
7. Gbur, G., and Wolf, E., "Relation between computed tomography and diffraction tomography," *J. Opt. Soc. Am.* **A 18**, No. 9, 2132-2137 (2001).
8. http://www.xradia.com/txmlt_desc.htm
9. Martz, Jr., H. E., "Validation of Radiographic Simulation Codes Including X-ray Phase-Effects for Mesoscale Objects," submitted to *JOSA A*; Lawrence Livermore National Laboratory, Livermore, CA, UCRL-JRNL-218242-DRAFT (2005).
10. Schneberk, D.J., et al., "Dimensional Measurements of Three Tubes by Computed Tomography," Lawrence Livermore National Laboratory, Livermore, CA, UCRL-TR-207195 (2004).
11. Edwards, J., et al., "Laser-Driven Plasma Loader for Shockless Compression and Acceleration of Samples in the Solid State," *Phys. Rev. Lett.* **92**, no. 7, 075002 (2004).
12. Aufderheide III, M. B., et al., "Analysis and modeling of phase contrast radiography of gradient density laser targets," *submitted to 2006 Symposium on Radiation Measurements and Applications* (*SORMA XI*), University of Michigan, May 23-25, 2006.
13. Amendt, P. A., et al., "Hohlraum-Driven Ignitionlike Double-Shell Implosions on the Omega Laser Facility," *Phys. Rev. Lett.*, **94**, 065004 (2005).
14. Sain, J., et al., "Analysis Procedures for Double-Shell Target Concentricity and Wall Thickness," Lawrence Livermore National Laboratory, Livermore, CA, UCRL-TR- 220178 (2006).